Cellular components in tumor microenvironment of neuroblastoma and the prognostic value

Xiaodan Zhong [1, 2, 3], **Yutong Zhang** [2], **Linyu Wang** [1, 3], **Hao Zhang** [1, 3], **Haiming Liu** [1, 3], **Yuanning Liu** [Corresp. 1, 3]

[1] College of Computer Science and Technology, Jilin University, Changchun, Jilin, China

[2] Department of Pediatric Oncology, The First Hospital of Jilin University, Changchun, Jilin, China

[3] Key Laboratory of Symbolic Computation and Knowledge Engineering, Ministry of Education, Jilin University, Changchun, Jilin, China

Corresponding Author: Yuanning Liu
Email address: liuyn@jlu.edu.cn

Background: Tumor microenvironment (TME) contributes to tumor development, progression, and treatment response. In this study, we detailed the cell composition of the TME in neuroblastoma (NB) and constructed a cell risk score model to predict the prognosis of NB.

Methods: xCell score was calculated through transcriptomic data from the datasets GSE49711 and GSE45480 based on the xCell algorithm. The random forest method was employed to select important features and the coefficient was obtained via multivariate cox regression analysis to construct a prognostic model, and the performance was validated in another two independent datasets GSE16476 and TARGET-NBL.

Results: We found that both immune and non-immune cells varies significantly in different prognostic groups, and were correlated with survival time. The proposed prognostic cell risk score (pCRS) model we constructed can be an independent prognostic indicator for overall survival (OS) and event-free survival (EFS) (training: OS, HR 1.579, EFS, HR 1.563; validation: OS, HR 1.665, 3.848, EFS, HR 2.203, all p-values < 0.01) and only independent prognostic factor in *International Neuroblastoma Risk Group* high risk patients (HR 1.339, 3.631; p-value 1.76e-2, 3.71e-5), rather than MYCN amplification. Besides, pCRS model showed good performance in grouping, in discriminating MYCN status, the area under the curve (AUC) was 0.889, 0.933, and 0.861 in GSE49711, GSE45480, and GSE16476, respectively. In separating high risk groups, the AUC was 0.904 in GSE49711.

Conclusion: This study details the cellular components in the TME of NB through gene expression data, the proposed pCRS model might provide a basis for treatment selection of high risk patients or targeting cellular components of TME in NB.

Introduction

Neuroblastoma (NB) is the third leading malignant disease in children aged 0-14 years, accounts for 7% of pediatric malignant tumors and responsible for 15% cancer-related deaths(Maris et al., 2007). The outcomes for NB vary distinctly from case to case; to be specific, some patients have spontaneous regression without intervention or mild treatment, while others may harbor inferior outcomes even though they have received multimodel therapy, including intensive chemotherapy, surgery, stem cell transplantation, radiotherapy, and molecular therapy(Pinto et al., 2015).

The mechanism of spontaneous regression may be induced by the TrkA/NGF pathway, cellular immunity, as well as other alternative mechanisms in NB(Brodeur and Bagatell, 2014). Such spontaneous regression can be observed in melanoma, which is tightly related to immune response. Auslander N. and colleagues had constructed the predictor called IMPRES based on the theory to predict the response of melanoma to immune checkpoint blocking (ICB) treatment. In their study, the total area under the curve (AUC) was 0.83, which had outperformed the existing predictors(Auslander et al., 2018). As a matter of fact, the interaction between tumor and its microenvironment affects tumor biological behavior and the associated treatment response(Joyce. and Fearon., 2015; Sun, 2016). Immunocyte infiltration in tumor microenvironment (TME) is tightly correlated with clinical outcomes and treatment response of tumor(Fridman et al., 2012). Existing direct and indirect evidence demonstrates that both cells and extracellular matrix in TME contribute to the major hallmarks of tumor in NB(Borriello et al., 2016), especially for tumor progression and metastasis.

Studies regarding the effect of cells in TME on NB have been carried out over the past few years. For instance, Asgharzadeh S. et al(Asgharzadeh et al., 2012) proved that tumor-associated macrophages (TAMs) were more infiltrative in metastatic NB than in local tumors; besides, they suggested that the interactions between tumor cells and inflammatory cells played certain roles in the malignant phenotype and affected tumor prognosis. Additionally, the study by Hashimoto O.(Hashimoto et al., 2016) had carried out immunohistochemistry (IHC) on 41 patients and discovered that TAMs and cancer-associated fibroblast (CAF) were markedly correlated with unfavorable clinical outcomes. In addition, Hishiki T.(Hishiki et al., 2018) observed that the invariant NKT cells preferred to infiltrate the spontaneously differentiated and/or regressed NB, and they believed that iNKT cells potentially contributed to these courses.

Simultaneously, studies on tumor-infiltrating lymphocytes (TIL) have also been conducted. For instance, Mina M.(Mina et al., 2015) found that the elevated number of tumor-infiltrating T lymphocytes was correlated with superior survival. Zhang P.(Zhang et al., 2017) and Wei

34   J.S.(Wei et al., 2018) had analyzed the TARGET-NBL dataset in succession and proposed the

35   immune suppressive microenvironment in NB; nevertheless, the former believed that CD4+ T-

36   cells (Th2 subtype) were related to the favorable survival regardless of the MYCN status,

37   whereas the latter suggested that the enhanced activation of NK cells, cytotoxic T lymphocytes

38   (CTL), and cytolytic signatures were associated with superior survival.

39   Moreover, some researchers have developed some algorithms to predict the fractions of cell

40   types, especially for immunocytes using transcriptomics data(Finotello and Trajanoski, 2018).

41   Among these computational approaches, the CIBERSORT(Newman et al., 2015) has been

42   widely used to evaluate the immune infiltration of human cancers(Waks et al., 2019; Wei et al.,

43   2018; Zhang et al., 2017; Zhou et al., 2019). Typically, CIBERSORT can achieve high accuracy

44   in calculating the immune cell infiltration of human cancers based on the microarray data;

45   however, it can not reflect all cell types of bulk tumors. On the other hand, xCell(Aran et al.,

46   2017) score algorithm can assess the abundance scores of 64 cell types based on single-cell gene

47   set enrichment analysis (ssGSEA), while the abundance scores can be obtained across both

48   microarray data and RNA-sequencing data.

49   Therefore, to elucidate the cell components of TME in NB, the xCell score algorithm was

50   employed based on the gene expression data of four independent datasets to portray the cell

51   components within the NB environment. Our results suggested that cell composition was

52   different in NB microenvironment with different prognosis, and cell types were associated with

53   the survival time. Also, a novel model was constructed in this study to provide a more powerful

54   biomarker for predicting the outcomes of NB patients.

55   ## Materials and Methods

56   **Data source and processing**

57   Gene expression profiles and clinical data were downloaded from GEO datasets

58   (https://www.ncbi.nlm.nih.gov/geo/ GSE49711, GSE45480 (GPL16876), and GSE16476) and

59   the TARGET-NBL data matrix (https://ocg.cancer.gov/programs/target/data-matrix). The

60   survival data of GSE49711 and GSE16476 were acquired from the R2 database

61   (https://hgserver1.amc.nl/cgi-bin/r2/ main.cgi). Specifically, a total of 149 NB patients were

62   included in the TARGET-NBL dataset, while 498 were in GSE49711 containing both RNA-seq

63   and clinical data, 649 were included in GSE45480, and 88 were in GSE16476 possessing both

64   microarray gene expression profile and clinical data. Table S1 has summarized the details of

65   baseline patient characteristics in four datasets. GSE49711 and GSE45480 datasets were the

66   training sets, while GSE16476 and TARGET-NBL were the validation cohorts.

Cell type enrichment abundance analysis based on gene expression data

68   The cell type enrichment score (xCell scores) was calculated based on the gene expression data

69   using the xCell(Aran et al., 2017) web tool (http://xcell.ucsf.edu/). Notably, the xCell tool

70   provides 64 cell types, including immunocytes, stromal cells, stem cells, and other cells; besides,

71   it recruits 10808 genes as the signatures to identify cell types. In this study, the gene names in the

72   four datasets were harmonized with the gene list provided by the xCell tool.

Subgroup analysis

74   In view of the clinical data contained included in the four datasets and the known risk factors

75   influencing NB patient survival, patients were classified into high-risk (HR) and non-high-risk

76   (NHR) groups, together with MYCN-amplified (MYCN-A) and MYCN-non-amplified (MYCN-

77   NA) groups. The xCell scores of immunocytes (including aDC, Th cells, cDC, NKT, Basophils,

78   macrophages M1, and CD8+ T-cells) and non-immunocytes (such as smooth muscle cells, HSC,

79   neurons, osteoblasts, endothelial cells, MSC, and fibroblasts) in different subgroups were

80   compared and displayed.

Random forest feature selection and risk score model

82   Patients were classified into two groups according to progression disease (unfavorable in

83   GSE49711, n=91, and stage 4 in GSE45480, n=214) or regression disease (favorable in

84   GSE49711, n=181, and stage 4s in GSE45480, n=78). Hereafter, the random forest model(Wang

85   et al., 2016) was adopted to select cell types for discriminating the two distinct groups, then

86   mean decrease Gini (MDG) and mean decrease accuracy (MDA) was used as the parameters to

87   estimate the importance. Two in three of the samples were randomly selected as training, and the

88   rest were as test to evaluate the importance and the out-of-bag (OOB) value, this step was

89   repeated for 100 times, an average of MDG, MDA, and OOB was as the final result.

90   Simultaneously, the coefficient was obtained through multivariate Cox regression analysis, and

91   the prognostic cell risk score (pCRS) model was constructed(Zhong et al., 2018). Patients were

92   classified into high- and low-risk score groups based on the average pCRS value.

K-means and hierarchical clustering

94   156 genes of the MYCN-157 signature(Valentijn. et al., 2012) (FAM85A was missing) were

95   picked up, and k-means clustering was utilized to divide the 498 patients into

96   MYCN_Signagure_Positive (MYCN_Sig_POS) or MYCN_Signature_Negative

97   (MYCN_Sig_NEG) group. In addition, hierarchical clustering was performed to distribute these

98   498 patients according to the xCell score of 64 cell types, together with the selected parameters

99   'binary' and 'ward.D2'.

100   **Statistical analysis**

101   The IBM SPSS version 23, Graphpad Prism 5, and R software were used for all statistical

102   analyses. Kaplan-Meier method and log-rank test were carried out to plot and compare the

103   survival curves. The xCell score or risk score of different groups was compared through the

104   Mann-Whitney U test. A two-tailed p-value of < 0.05 was considered as statistically significant.

105   # Results

106   **Cell components in TME of NB**

107   The final xCell abundance score was tightly correlated with the true cell proportions; as a result,

108   the former was approximated to represent the cell fraction in bulk tumor of NB. It was

109   discovered that in the four NB datasets, immunocytes made up at least one-half of the cell

110   components, followed by stromal cells (Fig. 1A). Compared to MYCN-NA group, MYCN-A

111   patients had fewer immunocytes while more stromal cells. In lymphoid cells, Th and NKT cells

112   had higher xCell scores in most datasets, whereas DC in myeloid cells, especially aDC, had a

113   higher xCell score (Fig. 1B, C). Besides, in the four datasets, neurons and stromal cells (such as

114   MSC, smooth muscle cells, osteoblasts, and endothelial cells) also had higher xCell scores (Fig.

115   1D).

116   **Subgroup analysis of cell type abundance**

117   Cell types were distinct among different prognostic groups. In GSE49711 and GSE45480,

118   patients were divided into different groups according to the risk factors involved in risk

119   stratification(Pinto et al., 2015) of NB, as presented in Fig. 1C, D and Fig. S1, Th cells had

120   markedly higher xCell scores in unfavorable prognostic groups; by contrast, DCs, NKT, and

121   CD8+ T cells had much higher xCell sores in favorable prognostic groups. In terms of the

122   stromal cell components, smooth muscle cells and osteoblasts possessed obviously higher xCell

123   scores in worse prognostic groups, while neurons had opposite results. Moreover, HSCs

124   displayed higher xCell scores in favorable prognostic groups. Similar results were found in

125   different INSS stages (Fig. S1C). On the other hand, survival analysis revealed that, the cell

126   abundance of NKT, aDC, cDC, CD8+ T cells, and neurons was positively correlated with long-

127   term survival; while Th1 cells, Th2 cells, smooth muscle cells, and osteoblasts were negatively

128   correlated with survival (Table S2, all p-values < 0.0001).

129   pCRS could serve as the independent prognostic factor

130   The random forest model was employed to select important features. A total of ten cell types

131   were involved after considering the xCell score and the importance of cell types in

132   discriminating groups. After repeating the random forest algorithm for 100 times, the average of

133   the OOB value was 11.22% in GSE49711 and 18.32% in GSE45480, respectively. Among them,

134   seven cell types were picked out as the signature involved in the risk score model. The parameter

135   MDG and MDA are shown in Fig. 2. The pCRS model was constructed, and the coefficient was

136   obtained according to the multivariate Cox regression analysis (Table S3). pCRS score = -

137   7.825*NKT+4.942*Th1+2.776*Th2+6.31*MSC-29.11*Neurons+9.285*

138   Osteoblasts+5.185*Smooth muscle. Multivariate Cox regression analysis in GSE49711

139   confirmed that the pCRS and high risk were the independent prognostic indicators for

140   unfavorable OS and EFS, among which, pCRS had a more significant p-value (Table S4).

141   Subsequently, the pCRS model was incorporated into subgroup analysis of GSE49711, including

142   high risk, INSS stage4, age > 18 months, and MYCN non-amplified, and the results suggested

143   that patients with higher pCRS value had remarkably shorter survival time in subgroups (all p-

144   values < 0.001) (Fig. 3).

145   Correlation of pCRS with the recognized prognostic molecules and immune markers

146   Correlation analysis indicated that ERCC6L was positively correlated with pCRS, with the

147   coefficient of up to 0.8112 and the p-value < 2.2e-16. In addition, the mRNA expression of

148   MYCN oncogene was also positively correlated with pCRS. On the contrary, the expression of

149   UBE4B(Hugo et al., 2016; Zage et al., 2013), NTRK1(Brodeur and Bagatell, 2014; Hugo et al.,

150   2016), CDH1, and CD44(Hugo et al., 2016), the favorable outcome prognostic factors, was

151   negatively correlated with pCRS (Fig. S2).

152   Also, cytotoxic T lymphocytes(Jiang et al., 2018) (CTL, the average expression of CD8A,

153   CD8B, GZMA, GZMB, and PRF1), and the cytolytic score(Havel et al., 2019) (CYT, the

154   average of GZMA and PRF1) were used to represent the activity of effector T-cells, and their

155   correlation with pCRS was assessed. Our results revealed that pCRS was negatively correlated

156   with the two T-cell indicators (p<0.0001) (Fig. S2G, H).

157   Comparison with the MYCN-157 signature

158   MYCN amplification was found in nearly 25% of NB patients, which was associated with

159   unfavorable outcomes(Huang and Weiss, 2013; Maris et al., 2007). Valentijn L.J.(Valentijn. et

160   al., 2012) found that MYCN non-amplified patients with functional MYCN signature had a poor
161   prognosis, and such phenomenon was confirmed by another study(Wei et al., 2018). In this
162   present study, the same results were obtained in GSE49711 (Fig. 4A, B). Multivariate analysis
163   suggested that pCRS and MYCN-157 signature could serve as the independent prognostic factors;
164   however, pCRS was more significant (p-value: 7.58e-11 vs. 2.59e-4).

165   Moreover, hierarchical clustering was also employed to distribute 498 patients into five
166   clusters, and our results indicated that cluster C2 had the worst survival time (Fig. 4C).
167   Meanwhile, the pCRS value of MYCN_Sig_POS and cluster C2 were evidently higher than
168   those of other groups (p < 0.0001) (Fig. 4D, E).

169   **Validation in independent datasets**

170   The performance of the pCRS model was validated in another two independent datasets
171   TARGET-NBL and GSE16476. In TARGET-NBL and its high risk group, the age group,
172   MYCN status, histology, MKI, and pCRS were included for Cox analysis, and pCRS was found
173   to be the only independent prognostic factor for OS and EFS (p-value:1.76e-5, 9.7e-05 and
174   3.27e-3. Table S5 and Fig. 5). In GSE16476, pCRS and age group were recognized as the
175   independent prognostic indicators for OS (Fig. 6). In the high risk group of GSE49711 and
176   TARGET-NBL, pCRS also serves as the independent prognostic indicator (Table S6).
177   Whereafter, the grouping ability of pCRS was accessed, and the AUC in discriminating MYCN
178   status reached 0.889, 0.933, and 0.861 in GSE49711, GSE45480, and GSE16476, respectively.
179   In addition, the AUC in distinguishing the high risk in GSE49711 was 0.904 (Fig. 7A-D and
180   Table S7).

181   Notably, the p-value of the xCell was not taken into account in our analysis, which might
182   result in some bias. To confirm the performance of our model, the p-values of the 7 cell types
183   were averaged, and then survival analysis was carried out among the 199 samples, with the mean
184   p-value of < 0.1. Afterwards, these patients were divided into 4 groups based on the quartile of
185   pCRS, and our results demonstrated that the OS rate and EFS rate gradually decreased with the
186   increase in pCRS (p < 0.0001) (Fig. 7E, F).

Discussion

188   Clinical trials on targeting TME in NB have been carried out and the main strategies focus on
189   TME cells, the signaling pathways, and immunotherapy(Borriello et al., 2016). In this study, the
190   cell components in TME of NB were comprehensively estimated through a gene signature-based
191   method named xCell, using wide-ranging in silico analyses from a large set of samples. In

192   addition, both microarray and RNA-seq data were utilized to train and validate the performance
193   of the as-constructed model. Results of xCell score analysis suggested that both immune and
194   non-immune cell components of NB were markedly different among different prognostic groups
195   and that the cell components of TME in NB affected patient survival.

196   As a matter of fact, studies regarding the influence of immunocytes on NB development and
197   prognostic value have been implemented over the past ten years. However, most of these studies
198   have addressed only one or more of these immunocytes components[9-12], while little attention
199   is paid to the overall cell composition in TME. Furthermore, the prognostic value of Th cells in
200   different adults cancers has also been elaborated(Fridman et al., 2012). In this study, we found
201   that both Th1 and Th2 cells were correlated with poor outcomes of NB.

202   There are various cell types in TME of cancers, some cells play bodyguard roles, such as
203   NK cells and CTLs; some cells are "hijacked" and promote cancer progression, like endothelial
204   cells(Hanahan and Coussens, 2012), TAMs(Asgharzadeh et al., 2012; Hashimoto et al., 2016),
205   and CAFs(Hanahan and Coussens, 2012). Moreover, some cells, including osteoblasts and MSCs,
206   may enhance bone and bone marrow metastases(Ma et al., 2011; Timaner et al., 2019), which are
207   common in stage 4 NB patients. Pelizzo G.(Pelizzo et al., 2018) had isolated and characterized
208   the tumor-derived MSCs and proposed the potential role of MSCs in promoting tumor invasion
209   and metastasis. Additionally, some cells are tissue-specific, such as epithelial cells clustered in
210   bladder urothelial carcinoma, cervical carcinoma, head and neck squamous cell carcinoma, and
211   other epithelial-derived cancers. Such a phenomenon has been proven by the xCell
212   algorithm(Aran et al., 2017). Therefore, neurons are enriched in low-grade glioma and NB, and
213   their roles in tumors are just like what Dirks P.B. said, "neurons refuse cancer's advances"(Dirks,
214   2019). In our study, patients had favorable long-term survival with higher neuron xCell scores in
215   GSE49711.

216   Cell composition in TME varies depending on the cancer types. In this study, Th cells, DCs,
217   smooth muscles cells, and HSCs accounts for over 40% of all cell types in the TME of NB
218   among the 3 datasets, and we believed that the interactions across different cell types promoted
219   or inhibited tumor progression, thereby affecting tumor prognosis. Hence, a prognostic cell type
220   risk score model (pCRS) was constructed in this study, and the performance of our model was
221   validated in the following analysis.

222   In the high risk group of INRG staging system(Pinto et al., 2015), the current method was
223   unable to distinguish patients with different outcomes, and treatment response and survival time
224   of these patients were inconsistent as well. Our pCRS model was capable of separating these
225   patients with different survival, which might shed some light on treatment regimen selection.

226 The prediction ability of the model was validated in GSE16476 and TARGET-NBL high risk
227 group. Our results showed that the high-risk score group has the remarkably short OS and EFS,
228 which was superior to that of MYCN amplification. Taken together, the pCRS model might
229 serve as an independent prognostic indicator in all patients and subgroups.

230 According to our previous studies, ERCC6L might be a cancer-promoting molecule of NB,
231 which was evidently associated with poor prognosis. It was discovered that pCRS was positively
232 correlated with the mRNA levels of ERCC6L and MYCN, whereas negatively correlated with
233 those of favorable prognostic indicator genes, including UBE4B, NTRK1, CHD1, and CD44.
234 CD8+ cytotoxic T lymphocytes play a vital role in eliminating tumors, which lays the foundation
235 of immune checkpoint blocking therapy(Farhood et al., 2019; Jiang et al., 2018). Besides, our
236 model was negatively correlated with the cytolytic signatures CYT and CTL. These results are
237 consistent with our expectations.

238 MYCN-157 signature was identified through silencing MYCN in NB cells, and its high
239 expression was found to be correlated with poor outcomes, regardless of MYCN amplified or
240 non-amplified(Valentijn. et al., 2012; Wei et al., 2018), which was in line with our study.
241 Meanwhile, the MYCN-signature positive group had higher pCRS value than that of the negative
242 group, similar to our speculation. Furthermore, our model was validated in two independent
243 datasets, which could serve as an independent prognostic factor. For INRG high risk patients, our
244 model was the only independent prognostic indicator, which also had good performance in
245 grouping, with the AUC in discriminating MYCN status and high risk of > 0.86.

246 Some limitations should be noted in our study. Firstly, the p-value of xCell score was not
247 considered in our analysis because of the remarkably reduced sample size. However, 199
248 patients with the average p-value among seven cell types of < 0.1 in GSE49711, and the results
249 showed the survival time was decreased with the increase in pCRS. Noteworthily, the p-value of
250 xCell score should be taken into account if more cases can be included in future studies, and
251 more meaningful results may be obtained. Secondly, the results of cell components were derived
252 from in silico analysis, which were not validated via histopathology as a result of the limited
253 experimental conditions and sample acquisition difficulties. This may be taken into account in
254 our future work. Nevertheless, cell composition in TME might be considered for inclusion in risk
255 stratification and decision-making for optimal treatment.

Conclusions

257 Our study portrays the cellular composition in the TME of NB through in silico analysis,

---

258   providing a clue of targeting cellular components in the TME. The proposed pCRS model might

259   afford some information for the personalized treatment of neuroblastoma patients, especially for

260   high risk patients.

Acknowledgements

262   The authors would like to thank TCGA and GEO platform for providing the data.

263

References

265   Aran, D., Hu, Z., and Butte, A.J. (2017). xCell: digitally portraying the tissue cellular
266   heterogeneity landscape. Genome biology *18*, 220.

267   Asgharzadeh, S., Salo, J.A., Ji, L., Oberthuer, A., Fischer, M., Berthold, F., Hadjidaniel, M., Liu,
268   C.W., Metelitsa, L.S., Pique-Regi, R*., et al.* (2012). Clinical significance of tumor-associated
269   inflammatory cells in metastatic neuroblastoma. Journal of clinical oncology : official journal of
270   the American Society of Clinical Oncology *30*, 3525-3532.

271   Auslander, N., Zhang, G., Lee, J.S., Frederick, D.T., Miao, B., Moll, T., Tian, T., Wei, Z.,
272   Madan, S., Sullivan, R.J*., et al.* (2018). Robust prediction of response to immune checkpoint
273   blockade therapy in metastatic melanoma. Nature medicine *24*, 1545-1549.

274   Borriello, L., Seeger, R.C., Asgharzadeh, S., and DeClerck, Y.A. (2016). More than the genes,
275   the tumor microenvironment in neuroblastoma. Cancer letters *380*, 304-314.

276   Brodeur, G.M., and Bagatell, R. (2014). Mechanisms of neuroblastoma regression. Nature
277   reviews Clinical oncology *11*, 704-713.

278   Dirks, P.B. (2019). Making a commitment: neurons refuse cancer's advances. Nature
279   neuroscience *22*, 507-508.

280   Farhood, B., Najafi, M., and Mortezaee, K. (2019). CD8(+) cytotoxic T lymphocytes in cancer
281   immunotherapy: A review. Journal of cellular physiology *234*, 8509-8521.

282   Finotello, F., and Trajanoski, Z. (2018). Quantifying tumor-infiltrating immune cells from
283   transcriptomics data. Cancer immunology, immunotherapy : CII *67*, 1031-1040.

284   Fridman, W.H., Pages, F., Sautes-Fridman, C., and Galon, J. (2012). The immune contexture in

285   human tumours: impact on clinical outcome. Nature reviews Cancer *12*, 298-306.

286   Hanahan, D., and Coussens, L.M. (2012). Accessories to the crime: functions of cells recruited to
287   the tumor microenvironment. Cancer cell *21*, 309-322.

288   Hashimoto, O., Yoshida, M., Koma, Y., Yanai, T., Hasegawa, D., Kosaka, Y., Nishimura, N.,
289   and Yokozaki, H. (2016). Collaboration of cancer-associated fibroblasts and tumour-associated
290   macrophages for neuroblastoma development. The Journal of pathology *240*, 211-223.

291   Havel, J.J., Chowell, D., and Chan, T.A. (2019). The evolving landscape of biomarkers for
292   checkpoint inhibitor immunotherapy. Nature reviews Cancer *19*, 133-150.

293   Hishiki, T., Mise, N., Harada, K., Ihara, F., Takami, M., Saito, T., Terui, K., Nakata, M.,
294   Komatsu, S., Yoshida, H.*, et al.* (2018). Invariant natural killer T infiltration in neuroblastoma
295   with favorable outcome. Pediatric surgery international *34*, 195-201.

296   Huang, M., and Weiss, W.A. (2013). Neuroblastoma and MYCN. Cold Spring Harbor
297   perspectives in medicine *3*, a014415.

298   Hugo, W., Zaretsky, J.M., Sun, L., Song, C., Moreno, B.H., Hu-Lieskovan, S., Berent-Maoz, B.,
299   Pang, J., Chmielowski, B., Cherry, G.*, et al.* (2016). Genomic and Transcriptomic Features of
300   Response to Anti-PD-1 Therapy in Metastatic Melanoma. Cell *165*, 35-44.

301   Jiang, P., Gu, S., Pan, D., Fu, J., Sahu, A., Hu, X., Li, Z., Traugh, N., Bu, X., Li, B.*, et al.* (2018).
302   Signatures of T cell dysfunction and exclusion predict cancer immunotherapy response. Nature
303   medicine *24*, 1550-1558.

304   Joyce., J.A., and Fearon., D.T. (2015). T cell exclusion, immune privilege, and the tumor
305   microenvironment. SCIENCE *348*, 74-80.

306   Ma, M., Ye, J.Y., Deng, R., Dee, C.M., and Chan, G.C. (2011). Mesenchymal stromal cells may
307   enhance metastasis of neuroblastoma via SDF-1/CXCR4 and SDF-1/CXCR7 signaling. Cancer
308   letters *312*, 1-10.

309   Maris, J.M., Hogarty, M.D., Bagatell, R., and Cohn, S.L. (2007). Neuroblastoma. The Lancet
310   *369*, 2106-2120.

311   Mina, M., Boldrini, R., Citti, A., Romania, P., D'Alicandro, V., De Ioris, M., Castellano, A.,
312   Furlanello, C., Locatelli, F., and Fruci, D. (2015). Tumor-infiltrating T lymphocytes improve
313   clinical outcome of therapy-resistant neuroblastoma. Oncoimmunology *4*, e1019981.

314 Newman, A.M., Liu, C.L., Green, M.R., Gentles, A.J., Feng, W., Xu, Y., Hoang, C.D., Diehn,
315 M., and Alizadeh, A.A. (2015). Robust enumeration of cell subsets from tissue expression
316 profiles. Nature methods *12*, 453-457.

317 Pelizzo, G., Veschi, V., Mantelli, M., Croce, S., Di Benedetto, V., D'Angelo, P., Maltese, A.,
318 Catenacci, L., Apuzzo, T., Scavo, E*., et al.* (2018). Microenvironment in neuroblastoma:
319 isolation and characterization of tumor-derived mesenchymal stromal cells. BMC cancer *18*,
320 1176.

321 Pinto, N.R., Applebaum, M.A., Volchenboum, S.L., Matthay, K.K., London, W.B., Ambros, P.F.,
322 Nakagawara, A., Berthold, F., Schleiermacher, G., Park, J.R*., et al.* (2015). Advances in Risk
323 Classification and Treatment Strategies for Neuroblastoma. Journal of clinical oncology : official
324 journal of the American Society of Clinical Oncology *33*, 3008-3017.

325 Sun, Y. (2016). Tumor microenvironment and cancer therapy resistance. Cancer letters *380*, 205-
326 215.

327 Timaner, M., Tsai, K.K., and Shaked, Y. (2019). The multifaceted role of mesenchymal stem
328 cells in cancer. Seminars in cancer biology.

329 Valentijn., L.J., Koster., J., Haneveld., F., Aissa., R.A., Sluis., P.v., C., M.E., Broekmans.,
330 Molenaar., J.J., Nes., J.v., and Versteeg, R. (2012). Functional MYCN signature predicts
331 outcome of neuroblastoma irrespective of MYCN amplification. PNAS *109*, 19190-19195.

332 Waks, A.G., Stover, D.G., Guerriero, J.L., Dillon, D., Barry, W.T., Gjini, E., Hartl, C., Lo, W.,
333 Savoie, J., Brock, J*., et al.* (2019). The Immune Microenvironment in Hormone Receptor-
334 Positive Breast Cancer Before and After Preoperative Chemotherapy. Clinical cancer research :
335 an official journal of the American Association for Cancer Research.

336 Wang, H., Yang, F., and Luo, Z. (2016). An experimental study of the intrinsic stability of
337 random forest variable importance measures. BMC bioinformatics *17*, 60.

338 Wei, J.S., Kuznetsov, I.B., Zhang, S., Song, Y.K., Asgharzadeh, S., Sindiri, S., Wen, X., Patidar,
339 R., Najaraj, S., Walton, A*., et al.* (2018). Clinically Relevant Cytotoxic Immune Cell Signatures
340 and Clonal Expansion of T-Cell Receptors in High-Risk MYCN-Not-Amplified Human
341 Neuroblastoma. Clinical cancer research : an official journal of the American Association for
342 Cancer Research *24*, 5673-5684.

343 Zage, P.E., Sirisaengtaksin, N., Liu, Y., Gireud, M., Brown, B.S., Palla, S., Richards, K.N.,
344 Hughes, D.P., and Bean, A.J. (2013). UBE4B levels are correlated with clinical outcomes in

345   neuroblastoma patients and with altered neuroblastoma cell proliferation and sensitivity to

346   epidermal growth factor receptor inhibitors. Cancer *119*, 915-923.

347   Zhang, P., Wu, X., Basu, M., Dong, C., Zheng, P., Liu, Y., and Sandler, A.D. (2017). MYCN

348   Amplification Is Associated with Repressed Cellular Immunity in Neuroblastoma: An In Silico

349   Immunological Analysis of TARGET Database. Frontiers in immunology *8*, 1473.

350   Zhong, X., Liu, Y., Liu, H., Zhang, Y., Wang, L., and Zhang, H. (2018). Identification of

351   Potential Prognostic Genes for Neuroblastoma. Frontiers in genetics *9*, 589.

352   Zhou, R., Zhang, J., Zeng, D., Sun, H., Rong, X., Shi, M., Bin, J., Liao, Y., and Liao, W. (2019).

353   Immune cell infiltration as a biomarker for the diagnosis and prognosis of stage I-III colon

354   cancer. Cancer immunology, immunotherapy : CII *68*, 433-442.

Figure 1

Cell types in tumor microenvironment of neuroblastoma.

(A, B) Summary of cell types in four datasets. (C, D) xCell score of immunocytes and non-immunocytes in GES49711. ***denotes $p < 0.001$; ** denotes $p < 0.01$; * denotes $p < 0.05$.
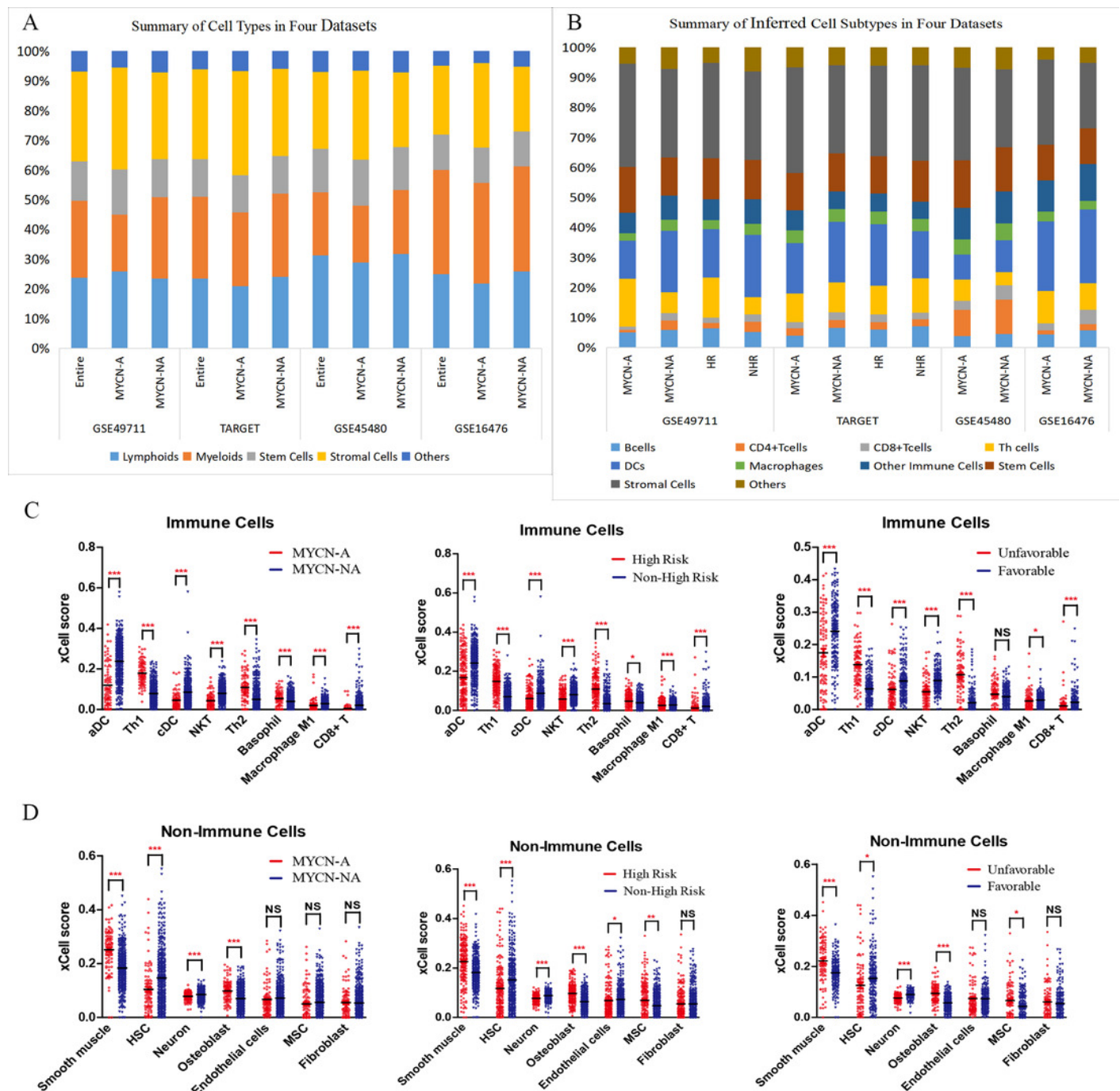
Figure 2

Importance of ten cell types in random forest algorithm.

(A) MDA and MDG in GSE49711. (B) MDA and MDG in GES45480. MDA: mean decrease accuracy; MDG: mean decrease Gini.
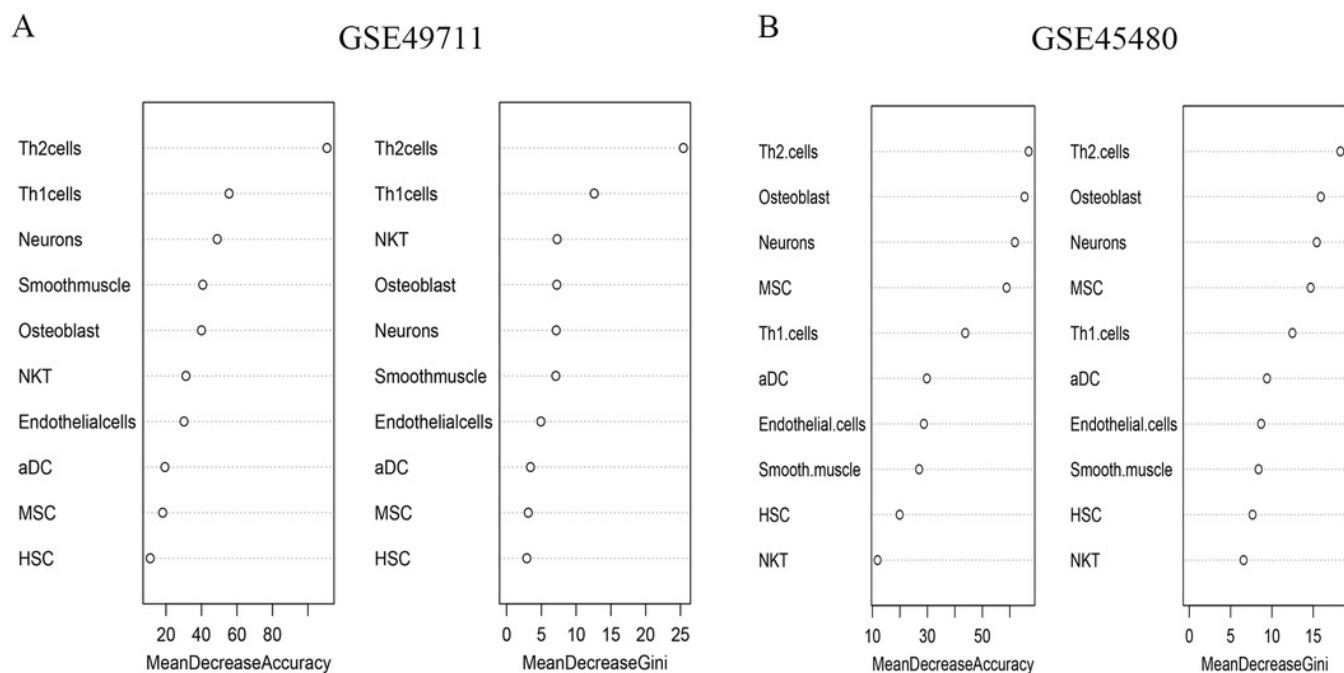
Figure 3

Kaplan-Meier plots of high/low pCRS value in GSE49711.

(A) OS. (B) EFS. (C-F) OS in high risk, stage 4, age > 18 months, and MYCN non-amplified. OS: overall survival; EFS: event-free survival.
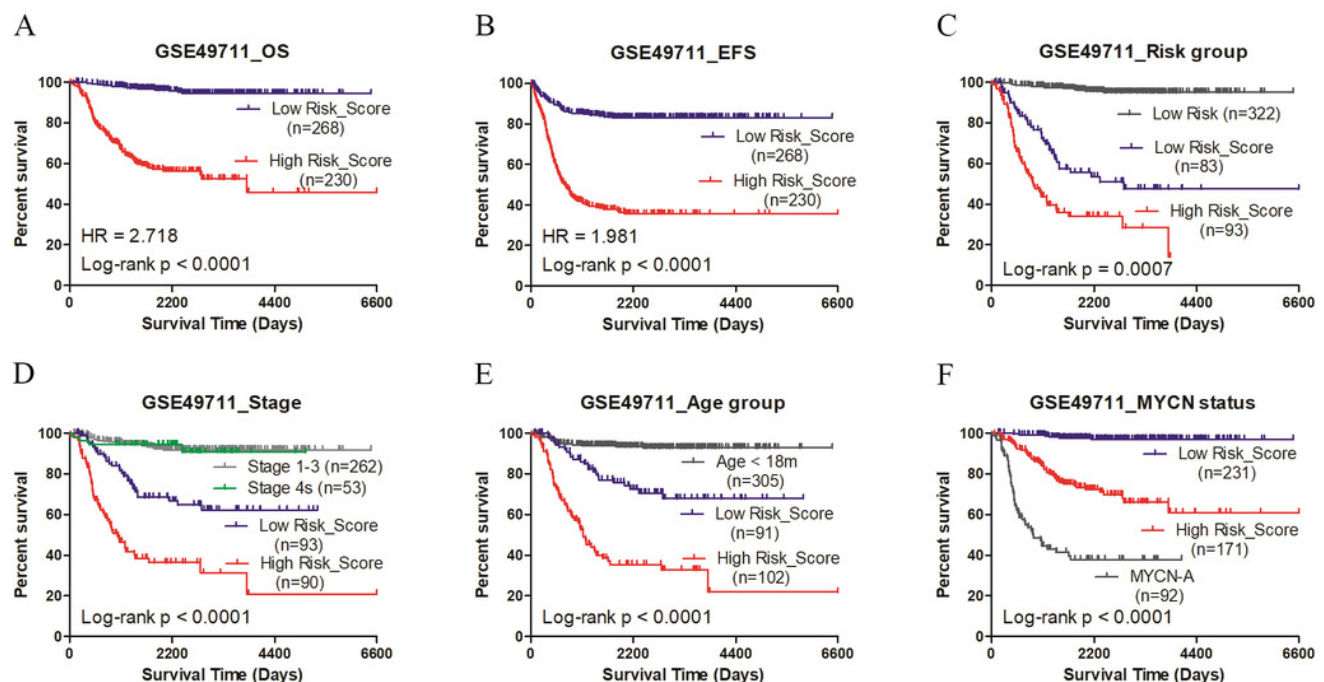
Figure 4

OS and pCRS of the MYCN-157 signature and clusters in GSE49711.

(A) OS of MYCN signature positive/negative. (B) OS of MYCN signature positive/negative without MYCN amplified. (C) OS of the clusters. (D, E) pCRS in different groups. OS: overall survival.
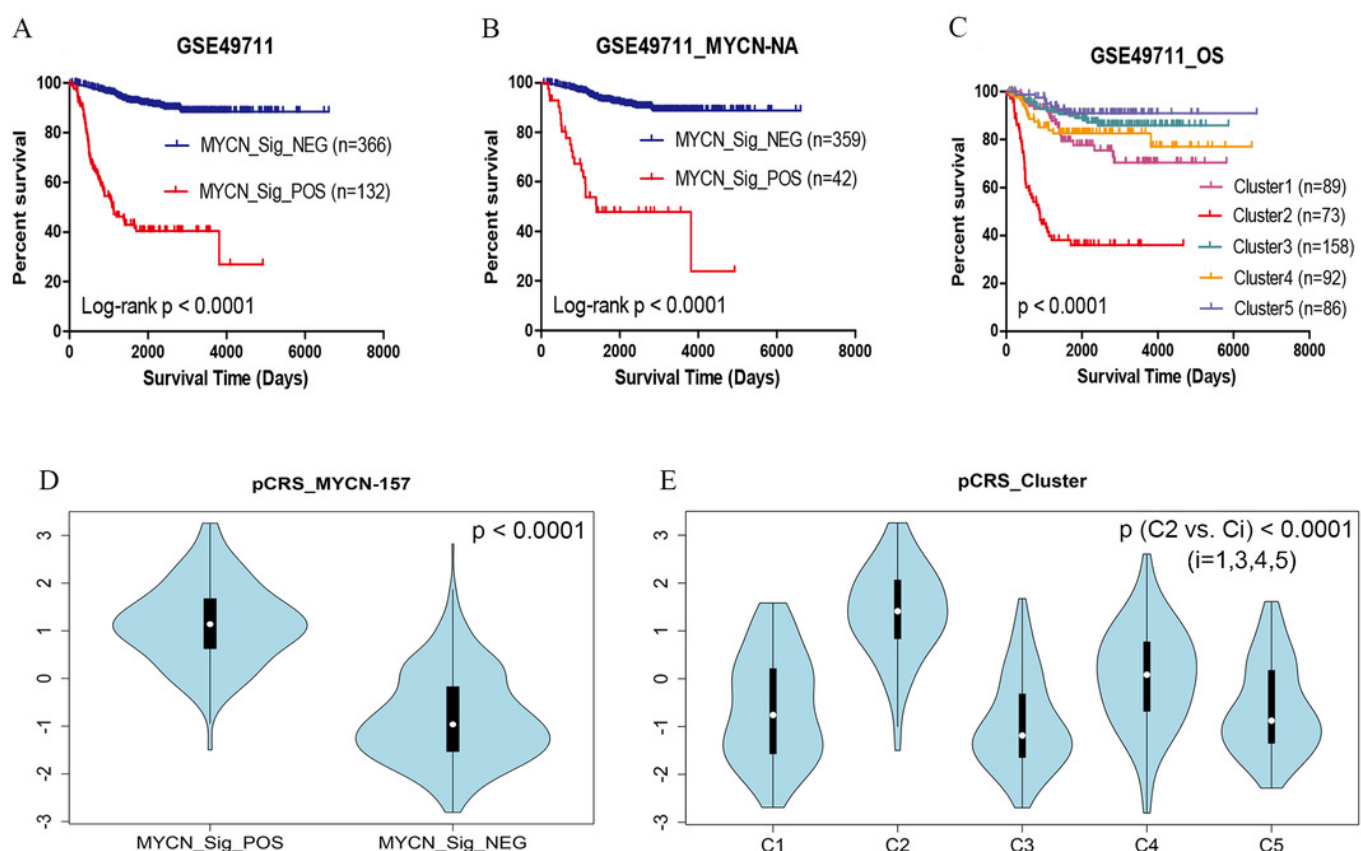
Figure 5

Kaplan-Meier plots of high/low pCRS score in TARGET-NBL.

(A) OS. (B-F) OS in high risk, unfavorable histology, stage 4, age > 18 months, and MYCN non-amplified. OS: overall survival.
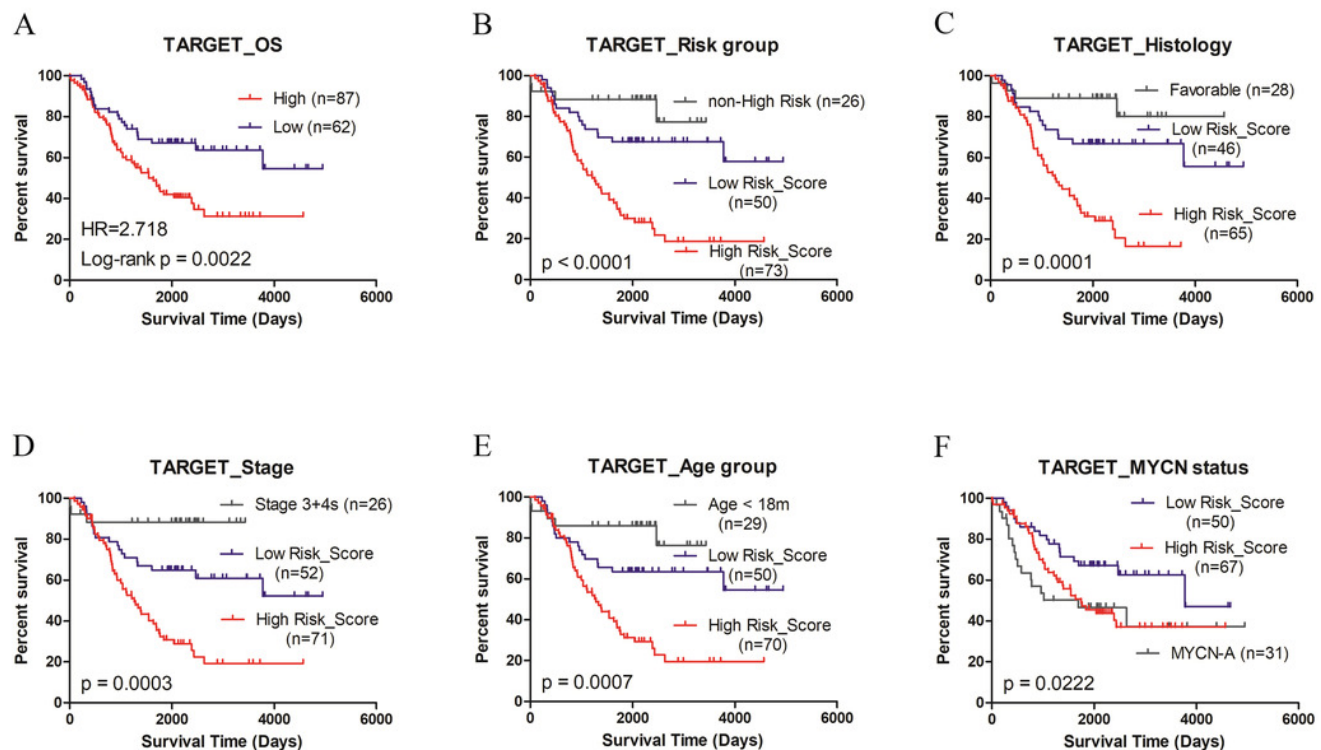
Figure 6

Kaplan-Meier plots of high/low pCRS score in GSE16476.

(A) OS. (B-D) OS in age > 18 months, MYCN non-amplified, and stage 4. OS: overall survival.
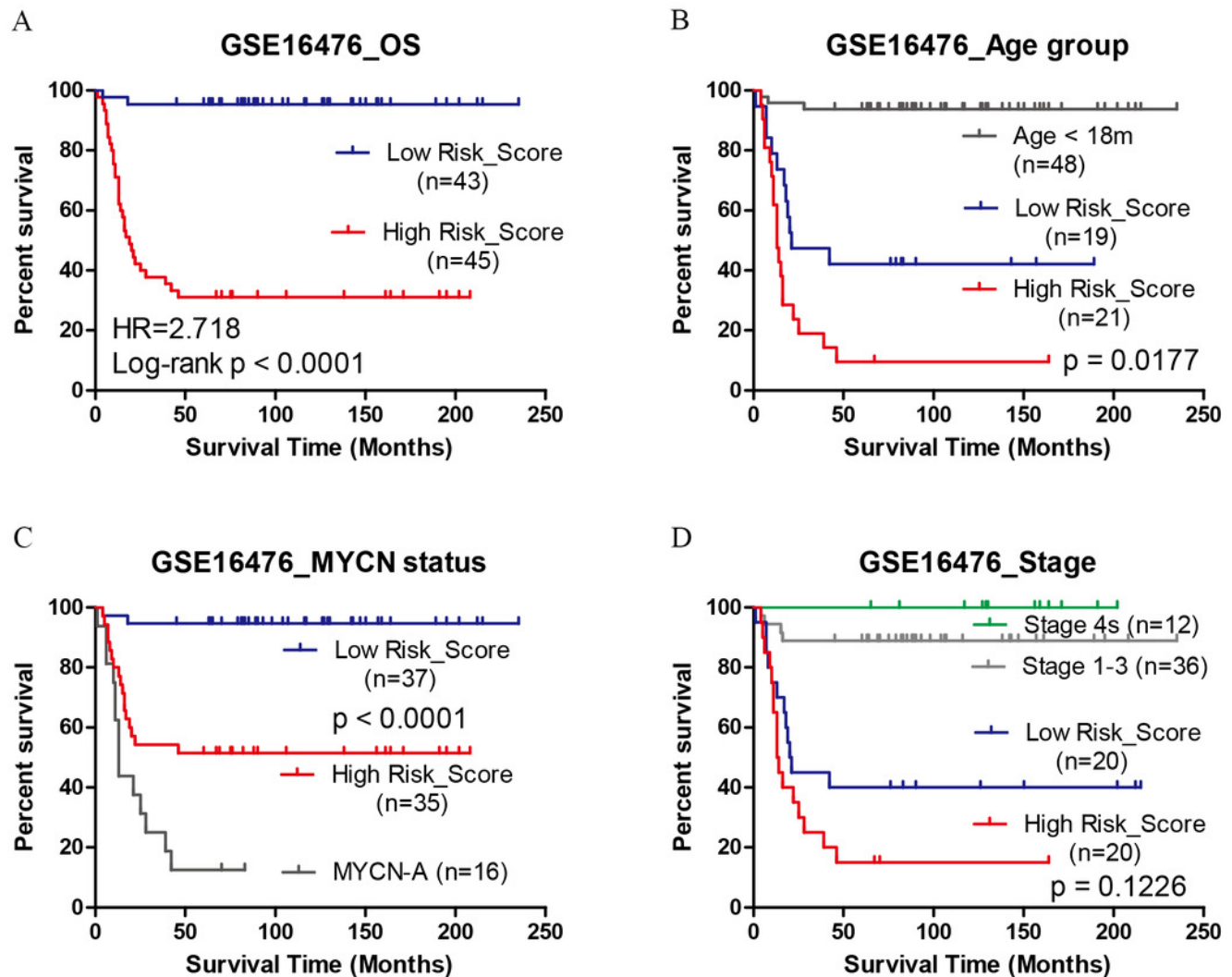
Figure 7

Performance in grouping of pCRS model.

(A-C) ROC of discriminating MYCN status in GSE49711, GSE45480, and GSE16476. (D) ROC of grouping high risk in GSE49711. (E, F) OS and EFS of patients considering p-value in GSE49711.
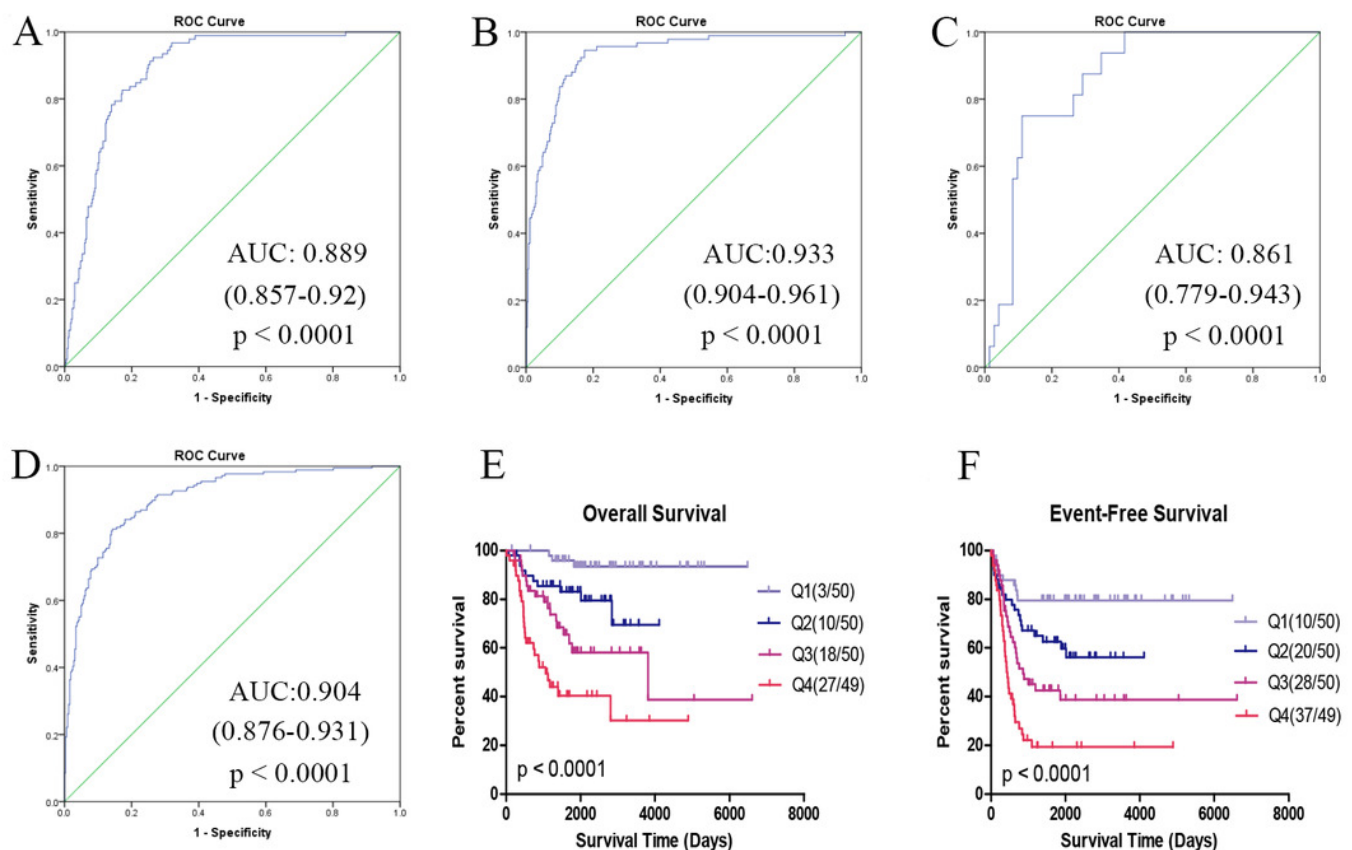
Multivariate Cox regression analysis in training and validation datasets.

Parameter	GSE49711			GSE16476			TARGET-NBL		
	HR	p-value	95% CI	HR	p-value	95% CI	HR	p-value	95% CI
pCRS	1.579	**4.70E-05**	1.267-1.967	1.665	**6.79E-03**	1.151-2.409	3.848	**1.76E-05**	2.08-7.118
Gender	0.629	**0.023**	0.421-0.938	1.147	0.71	0.558-2.356	0.856	0.591	0.485-1.51
Age group	1.543	0.185	0.813-2.930	4.638	**0.027**	1.193-18.032	0.939	0.958	0.091-9.666
MYCN status	0.935	0.948	0.127-6.914	1.249	0.558	0.593-2.632	1.639	0.157	0.826-3.252
High Risk	4.858	**7.25E-04**	1.943-12.149	NA	NA	NA	6.191	0.156	0.497-77.057
INSS stage	1.202	0.203	0.906-1.594	1.871	0.108	0.873-4.011	NA	NA	NA
Histology	NA	NA	NA	NA	NA	NA	1.417	0.721	0.209-9.594
MKI	NA	NA	NA	NA	NA	NA	1.236	0.254	0.859-1.778

2   HR: hazard ratio; CI: confidence interval. Bole type emphasizes p < 0.05.